12-15-2021

Numerical Modeling of Mineralizing Processes During the Formation of the Yangzhuang Kiruna-Type Iron Deposit, Middle and Lower Yangtze River Metallogenic Belt, China: Implications for the Genesis and Longevity of Kiruna-Type Iron Oxide-Apatite Systems

Xunyu Hu
China University of Mining and Technology

Simon Jowitt
University of Nevada, Las Vegas, simon.jowitt@unlv.edu

Feng Yuan
Hefei University of Technology

Guangxian Liu
East China Institute of Technology

Jinhui Luo
China University of Mining and Technology

See next page for additional authors

Repository Citation
Hu, X., Jowitt, S., Yuan, F., Liu, G., Luo, J., Chen, Y., Yang, H., Ren, K., Yang, Y. (2021). Numerical Modeling of Mineralizing Processes During the Formation of the Yangzhuang Kiruna-Type Iron Deposit, Middle and Lower Yangtze River Metallogenic Belt, China: Implications for the Genesis and Longevity of Kiruna-Type Iron Oxide-Apatite Systems. *Solid Earth Sciences* 23-37.
http://dx.doi.org/10.1016/j.sesci.2021.11.006

Available online at www.sciencedirect.com

ScienceDirect

Solid Earth Sciences 7 (2022) 23–37

www.elsevier.com/locate/SESCI

Numerical modeling of mineralizing processes during the formation of the Yangzhuang Kiruna-type iron deposit, Middle and Lower Yangtze River Metallogenic Belt, China: Implications for the genesis and longevity of Kiruna-type iron oxide-apatite systems

Xunyu Hu [a,b,*], Simon Jowitt [c], Feng Yuan [d], Guangxian Liu [e], Jinhui Luo [a,b], Yuhua Chen [a,b], Hui Yang [a,b], Keyue Ren [b], Yongguo Yang [a,b]

[a] *Key Laboratory of Coalbed Methane Resources & Reservoir Formation on Process, Ministry of Education, China University of Mining and Technology, Xuzhou 221008, China*

[b] *School of Resources and Geosciences, China University of Mining and Technology, Xuzhou 221116, China*

[c] *Department of Geoscience, University of Nevada Las Vegas, 4505 S, Maryland Pkwy, NV 89154-4010, USA*

[d] *School of Resources and Environmental Engineering, Hefei University of Technology, Hefei 230009, China*

[e] *East China University of Technology, Nanchang 330013, China*

Received 15 September 2021; revised 25 November 2021; accepted 25 November 2021
Available online 15 December 2021

Abstract

The Yangzhuang iron deposit is a Kiruna-type iron oxide-apatite (IOA) deposit within the Ningwu mining district of the Middle and Lower Yangtze River Metallogenic Belt (MLYRMB), China. This study applies a numerical modeling approach to identify the key processes associated with the formation of the deposit that cannot be easily identified using traditional analytical approaches, including the duration of the mineralizing process and the genesis of iron orebodies within intrusions associated with the deposit. This approach highlights the practical value of numerical modeling in quantitatively analyzing mineralizing processes during the formation of mineral deposits and assesses how these methods can be used in future geological research. Our numerical model links heat transfer, pressure, fluid flow, chemical reactions, and the movement of ore-forming material. Results show that temperature anomaly and structure (occurrence of the contact of intrusion and the Triassic Xujiashan group) are two key factors controlling the formation of the Yangzhuang deposit. This modeling also indicates that the formation of the Yangzhuang deposit only took some 8000 years, a reaction that is likely to be controlled by temperature and diffusion rates within the system. The dynamic changes of temperature and the distribution of mineralization also indicate that the orebodies located inside the intrusions most likely formed after magma ascent rather than representing blocks of existing mineralization that descended into the magma as a result of stoping or other similar processes. All these data form the basis for future research into the forming processes of Kiruna-type IOA systems as well as magmatic–hydrothermal systems more broadly, including providing useful insights for future exploration for these systems. The simulation approach used in this study has several limitations, such as oversimplified chemical reactions, uncertainty of pre-metallogenic conditions and limitation of 2D model. Future development into both theories and methods will definitely improve the practical significance of numerical simulation of ore-forming processes and provide quantitative results for more geological issues.

Keywords: Yangzhuang Kiruna-type deposit; Middle and Lower Yangtze River Metallogenic Belt; Numerical modeling; Duration of ore formation; Metallogenesis

* Corresponding author. Key Laboratory of Coalbed Methane Resources & Reservoir Formation on Process, Ministry of Education, China University of Mining and Technology, Xuzhou 221008, China.

E-mail address: xunyu.hu@cumt.edu.cn (X. Hu).

Peer review under responsibility of Guangzhou Institute of Geochemistry.

https://doi.org/10.1016/j.sesci.2021.11.006

1. Introduction

Kiruna-type iron oxide-apatite (IOA) deposits are high grade and economically important magmatic-hydrothermal mineral deposits that contain generally magnetite-dominated mineralization with apatite hosted by intermediate-felsic or volcanic-subvolcanic rocks (Hou et al., 2011; Nyström and Henriquez, 1994). Several Kiruna-type deposits have been discovered, including the Kiirunavaara deposit in the Kiruna area of northern Sweden (Förster and Knittel, 1979; Frietsch and Perdahl, 1995), the Shaytor deposit (Esmailiy et al., 2016) and the Chadormalu deposit (Heidarian et al., 2017) in Iran, the El Laco deposit (Sillitoe and Burrows, 2002) and El Romeral deposit (Rojas et al., 2018) in Chile, the Abagong deposit (Chai et al., 2013) and the Yangzhuang deposit (Ningwu Research Group, 1978) in China, with the latter forming the focus of this study. The processes involved in the formation of Kiruna-type deposits are thought to be extremely complex and are controlled by multiple coupled physical and chemical processes, which include fluid-flow, heat transfer, pressure variations, the migration of metals and ligands, and chemical reactions. All of these processes affect each other within a fully coupled system during the entirety of formation of mineral deposit (Ord et al., 2012). This means the factors that control the spatial distribution of iron mineralization, the mineralizing processes that operate in these deposits, and the factors associated with the formation of iron mineralization within intrusive bodies all remain unclear (Liu et al., 2010a, 2010b; Zou et al., 2017). Numerical simulation can provide insights into all of these processes while also generating quantitative results (Weis et al., 2012; Zou et al., 2017; Hu et al., 2020a) that could only be qualitatively or semi-quantitatively explained using traditional analytical techniques.

Advances in computer hardware and computational geoscience have enabled the development of advanced techniques for prospectivity modeling to be used in exploration for various types of mineral deposits as well as the numerical modeling of complex and coupled geological processes (Cheng, 2021). Unlike prospectivity modeling aimed at future mineral exploration (e.g., Porwal and Carranza, 2015; Li et al., 2015; Hu et al., 2018; Sun et al., 2019, 2020; Mao et al., 2020; Xiao et al., 2021; Zuo et al., 2021; Li et al., 2021; Liu et al., 2021; Chen et al., 2021; Zhang et al., 2021), numerical modeling provides insights into geological and metallogenic processes, furthering our understanding of these processes at both regional (Hobbs et al., 2007; Zhao et al., 2009; Ord et al., 2010; Zhao, 2015, 2016; Gorczyk et al., 2013; Gorczyk and Vogt, 2015; Li and Xu, 2015) and deposit (Zhao et al., 2008, 2018; Weis et al., 2012; Zou et al., 2017; Li et al., 2019; Zhu and Chen, 2019; Hu et al., 2019, 2020a, 2020b, 2022; Xiao and Wang, 2021) scales.

Recent research focused on the spatial distribution of mineralization within hydrothermal mineral deposits indicates that IOA-type mineralization within the MLYRMB is generally located within contact zones between intrusions and overlying units as well as along faults within the latter (Ningwu Research Group, 1978; Jin, 2014). However, the spatial distribution of iron mineralization within Kiruna-type IOA deposits and the factors that control this distribution remain somewhat poorly understood, with the processes involved in the genesis of some unusual IOA orebodies, such as those located within the intrusion associated with the Yangzhuang deposit, remaining uncertain. This study focuses on furthering our understanding of the key processes involved in the formation of this type of IOA deposit using a numerical simulation approach using COMSOL Multiphysics software, which allows us to set distributed ordinary differential equations and define formulas to conduct calculation. This approach could realize the numerical calculation of the complex and coupled processes that are associated with the formation of the Yangzhuang Kiruna-type IOA deposits and produce continuous numerical results to explore the forming processes of the deposit.

The Yangzhuang deposit is a typical Kiruna-type IOA deposit that discovered in the Ningwu volcanic basin of the MLYRMB, China (Ningwu Research Group, 1978). However, although both research and exploration has been undertaken on the deposit and the surrounding area, the factors controlling the spatial distribution of mineralization within the Yangzhuang deposit still remain somewhat unclear. In addition, some of the orebodies that define the deposit are located within the intrusion, somewhat unusual for typical Kiruna-type deposits. Previous research suggested that these orebodies originally formed at the contact between the intrusion and the surrounding country rock before stoping caused this dense mineralization to fall into the intrusion prior to the cooling and solidification of the latter (Jin, 2014) although this model lacks significant supporting evidence. All of this means the Yangzhuang deposit an ideal study area for numerical simulation of its forming processes, which can further our understanding of the genesis of Kiruna-type deposits. This study aims to investigate the following questions, namely: (1) what was the duration of the formation of the IOA mineralization within the Yangzhuang deposit, (2) what are the key controlling factors in the formation of the IOA-type Yangzhuang deposit, and (3) what processes generated the mineralization within the intrusion associated with the Yangzhuang deposit?

2. Geology of the Yangzhuang deposit

2.1. Regional geology

The MLYRMB (Fig. 1) hosts several world-class Cu–Fe polymetallic deposits and is one of the most important metallogenic belts in eastern China (Tang, 1998; Chang et al., 1991; Zhao et al., 2020; Zhai, 1992; Pirajno and Zhou, 2015; Zhou et al., 2020). This metallogenic belt is cut by a series of deep-seated and large faults, hosting eight large mining districts, which are the southeast Hubei, Jiurui, Anqing–Guichi, Luzong, Tongling, Nanling–Xuancheng, Ningwu, and Ningzhen mining districts (from west to east; Fig. 1; Modified from Zhou et al., 2020). These districts are dominated by porphyry–skarn copper-gold and magnetite–apatite IOA deposits along with other minor types of mineralization. The generation of these deposits are associated with three stages of

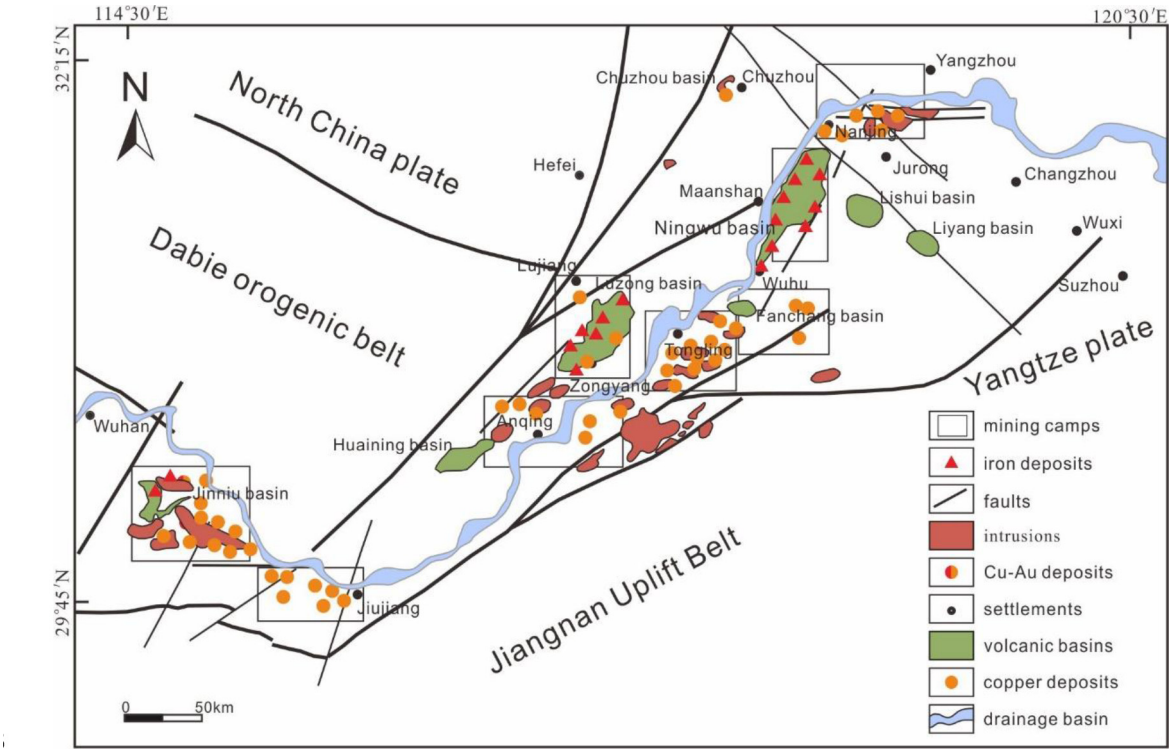

Fig. 1. Map showing the location of major volcanic basins and intrusions and associated IOA and copper deposits within the MLYRMB. Modified from Zhai (1992) and Zhou et al. (2020).

Mesozoic magmatism 149–135, 133–125 and 123–105 Ma (Zhou et al., 2015), all of which were driven by the evolution of this area during the associated Yanshanian tectonic event (Ningwu Research Group, 1978).

Most basins in this metallogenic belt are pull-apart basins trending N–S to NE–SW, hosting a group of intrusive and extrusive olivine latite units. These basins are associated with volcanic–subvolcanic hydrothermal–sedimentary polymetallic deposits that are similar to the Kiruna-type Kiirunavaara deposit in the Kiruna area of northern Sweden (Ningwu Research Group, 1978). The Ningwu mining district is in the northeastern MLYRMB. Two groups of faults controlled the formation of this mining district and form the basic structure of this district. The first group trends NNE–SSW and the second trends NW–SE. A train of volcanic units are hosted in this mining district, including the Triassic Zhouchongcun group, Huangmaqing groups and the Jurassic Xiangshan Group. Three orefields are defined within the Ningwu mining district, namely the Meishan, Aoshan and Zhonggu orefields (from north to south; Fig. 2).

2.2. Geology of the Zhonggu orefield

The Zhonggu orefield is seated in the south edge of the Ningwu mining district (Fig. 3). Two deep major faults, trending NNE–SSW and NNW–SSE, controlled the formation of the intrusive and extrusive magmatism (Fig. 3). The whole orefied is dominated by the Triassic Zhouchongcun group, Triassic Huangmaqing group and Jurassic Xiangshan groups, among which the former two have close temporal and spatial relationship with the formation of iron mineralization. All of the IOA-type mineral deposits in the Zhonggu orefield are linked with small hypabyssal to superhypabyssal intrusive bodies, which includes the Baixiangshan, Xiashan, Gushan, Youfanggai and the Yangzhuang porphyritic diorite intrusions (Hou et al., 2010).

2.3. Deposit geology

The Yangzhuang deposit locates in the southern side of the Zhonggu orefield and classified as an IOA deposit (Fig. 4; Mineral Explorating and Developing Bureau of Eastern China, 2011; Jin, 2014). The ore minerals within the deposit are dominated by magnetite (generated at the temperature range of 330 °C–500 °C, Li et al., 1979) with minor amounts of hematite, with the individual orebodies identified by drilling and geophysical detection (i.e., magnetic anomalies) generally located along the contact between the porphyritic diorite and the Xujiashan Group, within the Xujiashan Group itself, and within the porphyritic diorite. Two small domes controlled the formation of the intrusive unit in the Yangzhuang deposit. Most of the IOA mineralization in this area is formed from hydrothermal fluid derived from mantle magmas and spatially linked with a concealed porphyritic diorite (Wang et al., 2001). The contact between the intrusion and wall rocks is the main location for generation of the iron mineralization (Li et al., 2015). Intrusions in the Yangzhuang deposit are spatially controlled by folding and faulting, which formed the migration

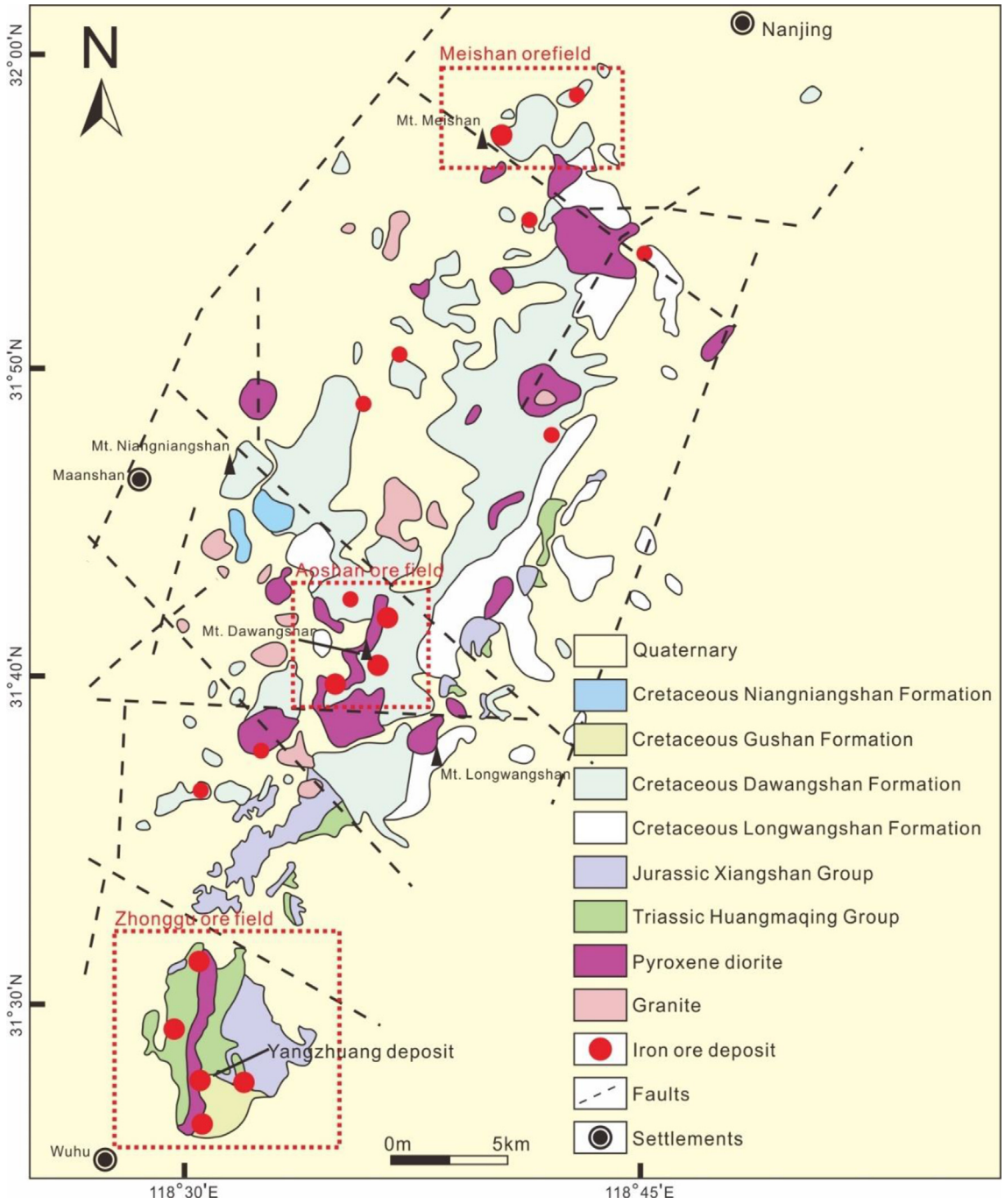

Fig. 2. Map showing the geology and several main mineral deposits of the Ningwu Basin; Modified from Ningwu Research Group (1978).

channels for magmas and generated several cupolas and stocks in appropriate locations. The main intrusion associated with iron mineralization is a porphyritic diorite, with some porphyritic felsite, porphyritic diorite, spessartine-bearing and gabbroic dikes in its surrounding locations.

3. Methods

There are typically three main steps in geoscientific numerical modeling, namely conceptual, mathematical, and simulation modeling (Zhao et al., 2009; Zou et al., 2017; Hu et al., 2020a). Here we improve this workflow and build conceptual, simplified, mathematical, and simulation models for the Yangzhuang deposit, which here is termed a four step of model workflow approach. The first step is to build a conceptual model from the knowledge of the metallogenic model and previous geological data available for the deposit. This model consists of the text describing the processes involved in metallogenesis and the formation of the deposit, sometimes with a diagram of a metallogenic model. The second step is to build a simplified model using the complex geological data available that describes the structure of the deposit. Those

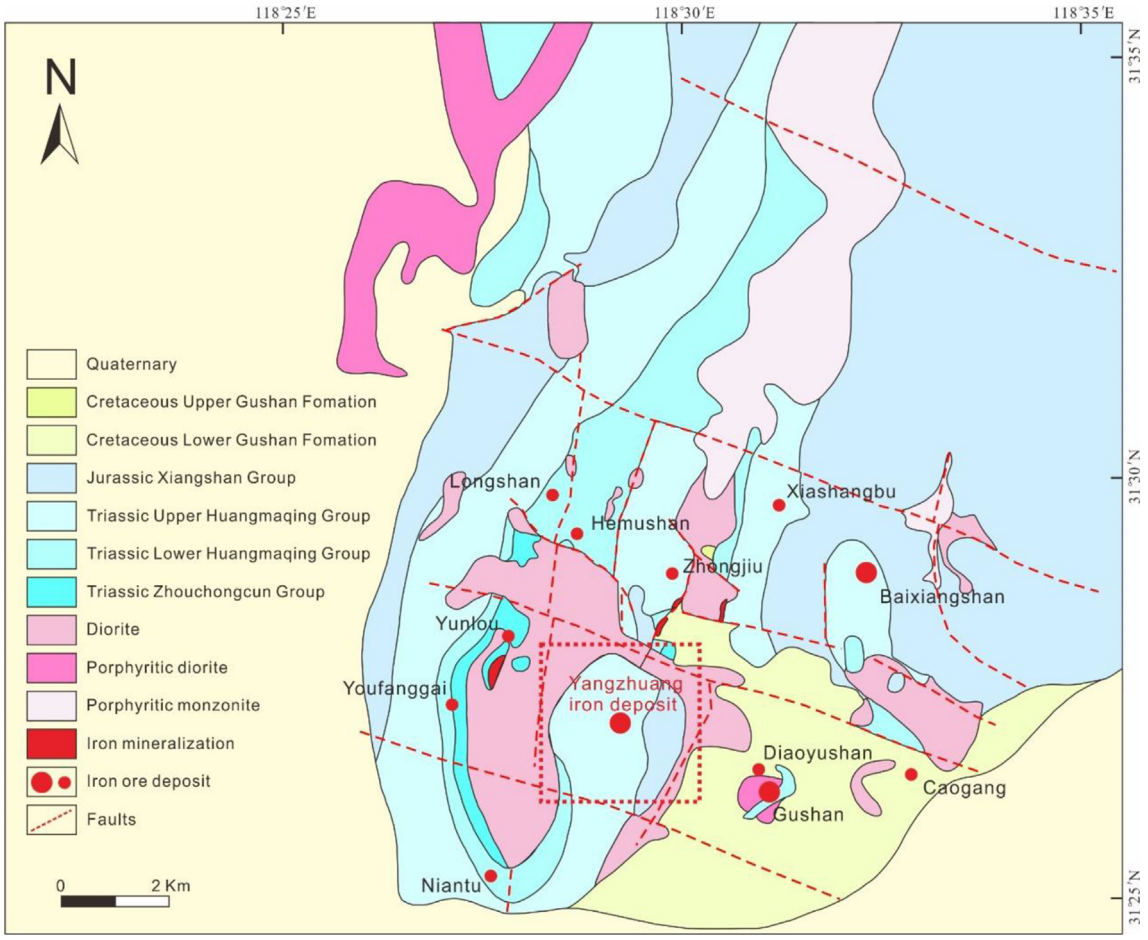

Fig. 3. Map showing the geology of the Zhonggu orefield and the location of most iron ore deposits. (Mineral Explorating and Developing Bureau of Eastern China, 2011).

unimportant details are typically omitted in order to highlight key structures and shapes, reducing the amount of calculations and computing power required. The third step is to combine a group of mathematical equations to describe the physical and chemical processes and their coupled relationships. The last step is to build a simulation model, including adjusting software configuration, assigning values to parameters, setting initial and boundary conditions and other operations. The workflow of the numerical simulation used in this paper is shown in Fig. 5.

3.1. Conceptual, simplified and simulation models for the Yangzhuang deposit

The conceptual model of the Yangzhuang Kiruna-type IOA deposit is based on the results of previous research on this and other similar deposits within the MLYRMB, combining the geological characteristics of this and other deposits (Jin, 2014; Hu et al., 2018) and the information shown along cross-section A-B in Fig. 4. The section shows that the iron orebodies are located within the contact zone between the intrusion and the overlying units and within the intrusion itself. Previous research suggests that the latter style of mineralization represents IOA orebodies that formed at the contact between the intrusion and the surrounding country rock but then stoped into the intrusion as a result of the density of the IOA mineralization (~4.5 t/m^3) prior to the cooling and solidification of the latter. Here we consider the results of previous research during our modeling of the Yangzhuang deposit, using a maximum depth of 4000 m and a width of 1300 m (Fig. 6b). Our modeling simulates changes of temperature of the intrusion to confirm whether any significant mass of mineralization could stope into the intrusion prior to sufficient cooling and solidification. This modeling sets the initial temperature of the intrusion as 1200 °C, higher than the solidification temperature of the intermediate–basic magmas in the study area. This is also much higher than the temperature of formation of the IOA mineralization within the Yangzhuang deposit, reflecting the fact that this igneous body must have been at a higher temperature than the ore-forming fluids derived from these magmas (Liu et al., 2011; Liu and Dai, 2014; Zou et al., 2017; Hu et al., 2019, 2020a, 2020b). Our previous research (Hu et al., 2019, 2020a) also indicates that the simulation of chemical reactions can only produce results with relative values (i.e., is only valid when used for comparison with other parts of the same model) as a result of a lack of knowledge of the

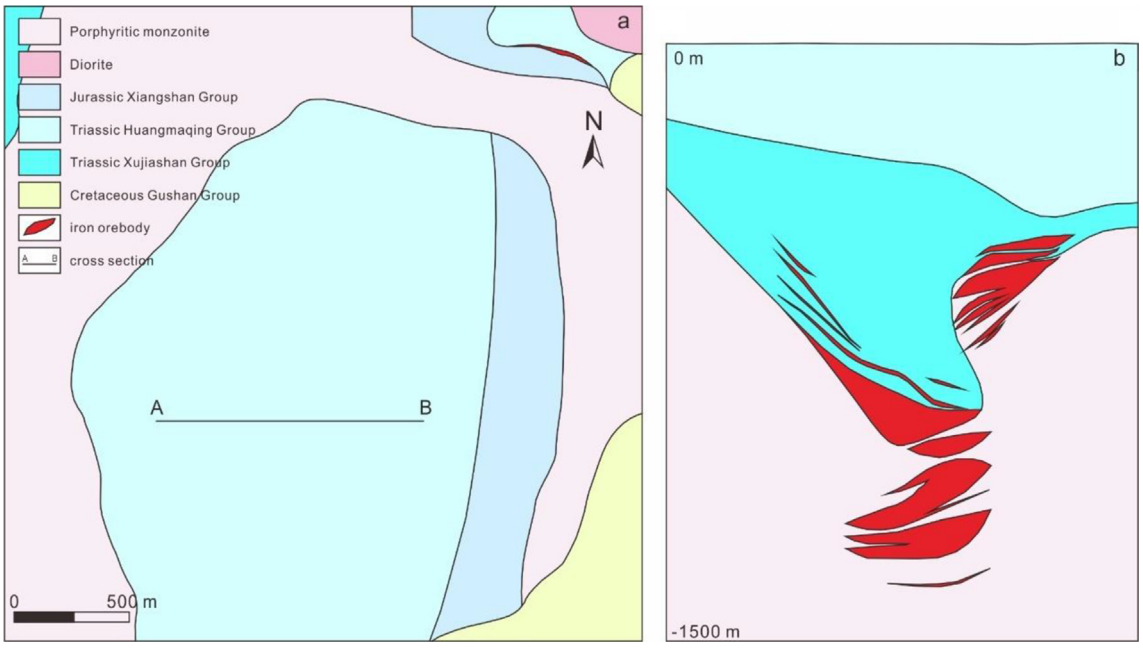

Fig. 4. (a) Map showing the geology of the Yangzhuang IOA deposit. (b) Cross-section through the deposit along A–B based on data from the Mineral Exploring and Developing Bureau of Eastern China (2011).

equilibrium constants of these chemical reactions. This knowledge means initial $Fe^{2+/3+}$ and O^{2-} concentrations were set to 0.05 mol/m^3 with $Fe^{2+/3+}$ located within the ore-forming fluids and O^{2-} within the overlying units. The other parts of the model have a temperature gradient of 25 °C/km with a surface temperature of 20 °C, reflecting average surface temperature conditions. Our model also incorporates a pressure gradient of 26.5 MPa/km, reflecting the average density of the rocks in this area and a surface pressure that is equal to atmospheric pressure. Our previous research also indicates that hydrothermal deposits tend to over timespans of 100,000 years or even 10,000 years (Hu et al., 2020a), meaning a calculation time of 10,000 years with a time step of 25 years was used during our modeling, with this model setup to yield transient results. The simulation model was constructed using the boundary conditions and conceptual model outlined above (Fig. 6) with relevant rock material parameters given in Table 1.

The temperature of the boundaries is the same as the geothermal gradient and the boundary pressure is the same as the lithostatic pressure gradient. The location for chemical reaction is far from the surface so we omitted the hydrostatic pressure during this modeling. As mentioned above, the values of the concentrations of reactants and products within the chemical reactions are only relative values with no practical

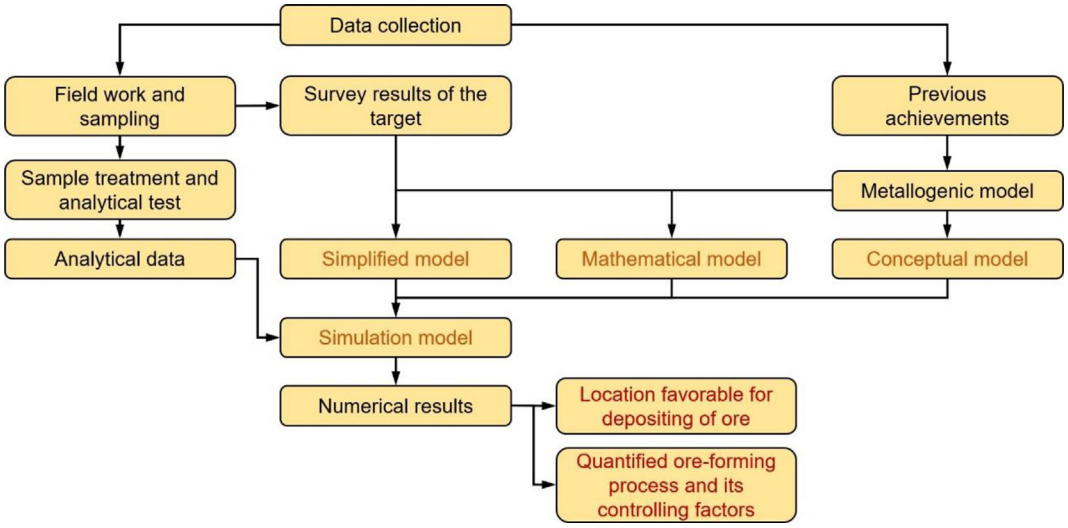

Fig. 5. Workflow used in the numerical modeling of the mineralizing processes associated with the formation of the Yangzhuang deposit; adapted from Hu et al. (2019, 2020a).

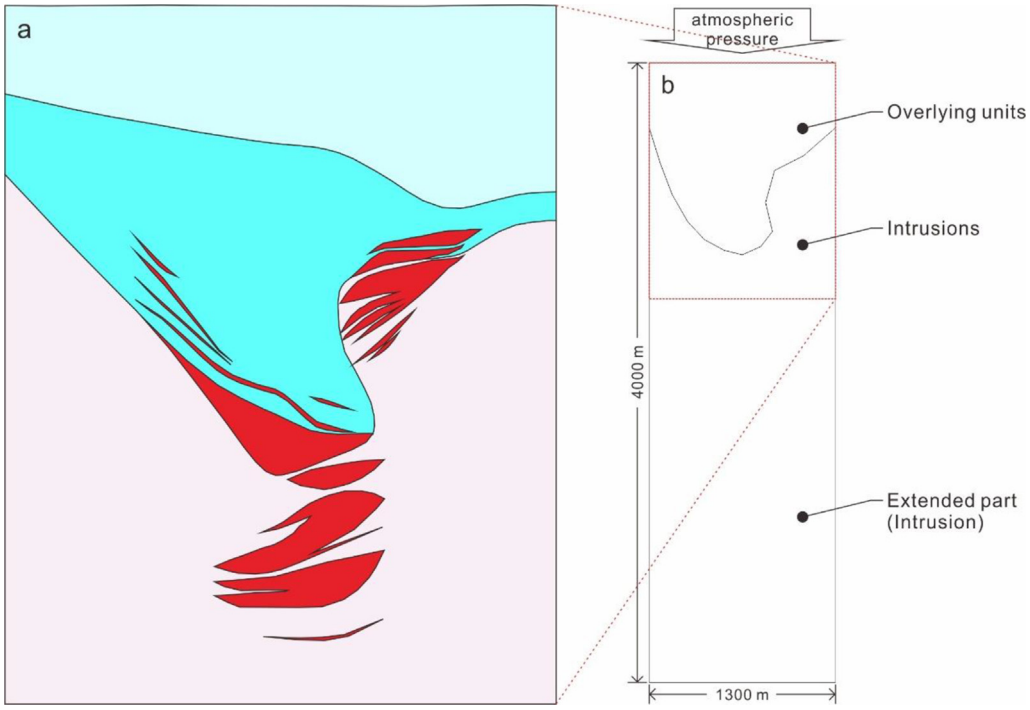

Fig. 6. Simulation model (b) used during our research built using the conceptual model described in the text and a comparison with the cross-section of the Yangzhuang deposit (a; from Fig. 4b).

Table 1
Material parameters used during the simulation of ore-forming processes of the Yangzhuang deposit; adapted from Mineral Explorating and Developing Bureau of Eastern China (2011) and Jia et al. (2018).

Rock type	Density (Kg/m^3)	Specific heat capacity (J/Kg/K)	Porosity (/1)	Permeability (10^{-12} m^2)	Heat conductivity (W/m/K)
Overlying unit	2650	820	0.23	6.0	3.1
Intrusions	2600	870	0.21	5.0	2.8

meaning as a result of a lack of knowledge of some variables, including the equilibrium constant of chemical reaction (Hu et al., 2020a). This means that the inlet concentration of $Fe^{2+/3+}$ within the intrusion was set as 0.05 mol/m^3 in the intrusion with 0 mol/m^3 in the overlying units, and the inlet concentration of O^{2-} was 0 mol/m^3 and 0.05 mol/m^3 in the intrusion and overlying units, respectively.

3.2. Mathematical modeling of the Yangzhuang deposit

The whole magmatic-hydrothermal system that formed the Yangzhuang deposit involves several physical and chemical processes which are controlled by fluid migration, heat transfer, pressure and stress, chemical reactions and material/solute migration. The coupled relationship of these processes is quite complex, as shown in Fig. 7. The main processes involved in our model are divided into five separate parts and their mathematical descriptions are given below.

(1) Geothermal/lithostatic temperature and pressure gradients

Geothermal and lithostatic pressure gradients are generated using the following two equations.

$$T = T_0 - y \bullet G_H \tag{1}$$

$$P = P_A - y \bullet G_L \tag{2}$$

where T is the initial value of the temperature of the model in °C, T_0 is normal room temperature (set as 20 °C under 1 atmospheric pressure, 1.013×10^5 MPa), y is the depth of the model in m and the top of the model is set as earth surface (i.e., the depth of the top is 0 m), G_H is the temperature gradient which is set as 25 °C/km (Bickle, 1978; Lister, 1963), P is pressure in MPa, P_A is the atmospheric pressure at the top (the surface, with depth = 0 m) of the model, G_L is the Lithostatic pressure gradient within the model (set as 26.5 MPa/km; adapted from Anderson, 1989; Hart et al., 1995; Hu et al., 2003).

(2) Heat transfer in porous media

The COMSOL software package has defined a group of default equations to describe the exchange of heat and the conservation of energy. The equations used in our model are given below:

$$d_z(\rho C_p)_{eff}\frac{\partial T}{\partial t} + d_z\rho C_p \nu \cdot \nabla T + \nabla \cdot \boldsymbol{q} = d_z Q + q_0 + d_z Q_{vd} \tag{3}$$

$$\mathbf{q} = -d_z k_{eff} \nabla T \tag{4}$$

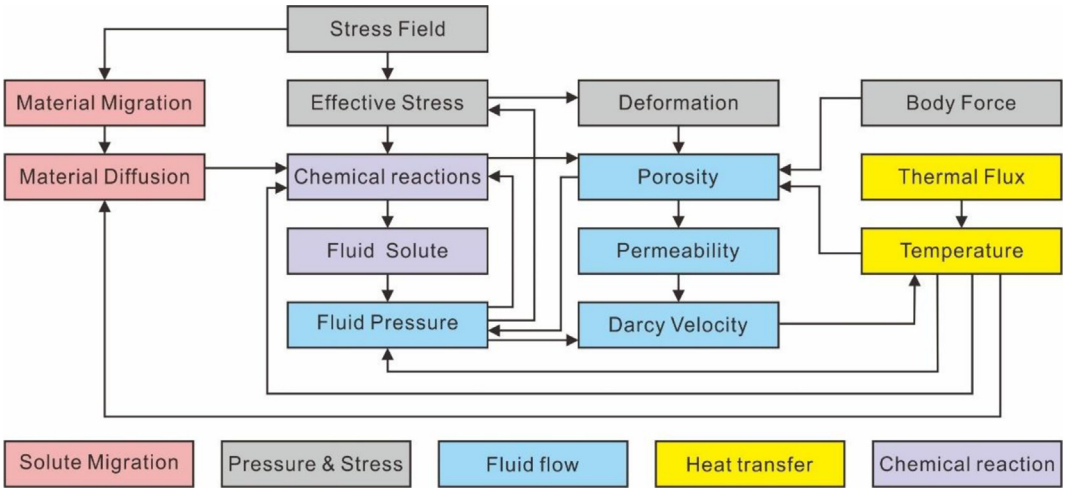

Fig. 7. The coupled relationships between all five individual process during mineralizing processes. Adapted from Hu et al. (2019, 2020a).

$$(\rho C_p)_{eff} = \theta_p \rho_p C_{p,p} + (1-\theta_p)\rho C_p \quad (5)$$

$$k_{eff} = \theta_{\mathrm{p}} C_{\mathrm{pr}} + (1-\theta_{\mathrm{p}}) C_m + k_{disp} \quad (6)$$

$$\theta_{\mathrm{p}} = 1 - \varepsilon \quad (7)$$

where d_z is the thickness of the model (Fig. 6b, set as 600 m), ρ is density of the hydrothermal fluid, C_p is the heat capacity of fluid mixed with chemical reactants and products, T is temperature of the model, t is time, ν is the velocity of fluid, $\mathbf{q}$ is total heat dissipation, q_0 is heat flux flowing into the model, Q is total heat generated/consumed during the chemical reaction, Q_{vd} is the heat transferred from the background (i.e., four sides, and the top and the bottom of the model), ρ_{p} is the density of porous medias (intrusion and sediments), θ_{p} is the volume fraction of porous media, $C_{p,\mathrm{p}}$ is specific heat capacity, k_{eff} is heat conductivity effective during the whole processes, C_{pr} is the heat conductivity of porous media, C_m is the heat conductivity of fluid mixed with chemical reactants and products, k_{disp} is the coefficient describing the heat dissipation to the background of the model, and ε is porosity of each intrusion and sediments.

(3) Fluid-flow

Fluid-flow in rock and intrusion is driven by the buoyancy provided by pressure gradient, which can be described using Darcy's law (Kumar et al., 2016; Mandl, 1988).

$$\nu = -\frac{k}{\mu}\nabla P + g\rho_l \quad (8)$$

$$Q_m = \frac{\partial}{\partial t}(\varepsilon\rho_l) + \nabla\cdot(\rho_l \nu) \quad (9)$$

where ν is the velocity, k is permeability, μ is viscosity, ε is porosity, Q_m is source/sink term, t is time, ∇P is pressure gradient, and $g\rho_l$ is combination of gravity of the geological units and fluid within the pore space, g is the gravitational constant (set as 9.8 m/s^2) and ρ_l is fluid density.

(4) Chemical reaction

Chemical reaction within our model is carried out within the temperature range from 330 °C to 500 °C (Li et al., 1979). A simplified equation is built to describe the formation of magnetite:

$$Fe^{2+} + 2Fe^{3+} + 4O^{2-} = Fe_3O_4 \quad (10)$$

We also use enthalpy and entropy variation equations to describe chemical reactions during ore-forming processes:

$$H_j = \sum_{i\in prod} co_{ij} h_i - \sum_{i\in react} (-co_{ij}) h_i \quad (11)$$

$$S_j = \sum_{i\in prod} co_{ij} s_i - \sum_{i\in react} (-co_{ij}) s_i \quad (12)$$

where H_j is enthalpy of the whole reaction, $\sum_{i\in prod} v_{ij}h_i$ is the sum of the enthalpy of reaction product (e.g., the enthalpy of Fe_3O_4 in this model), $\sum_{i\in react} (-v_{ij})h_i$ is the sum of the enthalpy of reactants ($Fe^{2+/3+}$ and O^{2-}), S_j is entropy of the whole reaction, $\sum_{i\in prod} v_{ij}s_i$ is the sum of the entropy of reaction product, $\sum_{i\in react} (-v_{ij})s_i$ is the sum of the entropy of reactants ($Fe^{2+/3+}$ and O^{2-}), all with units of J/(mol•K). Besides, co_{ij} is the coefficient of each reactant/product, which is determined by Eq. (10). i and j represent different materials participating in the reaction (e.g., $Fe^{2+/3+}$, O^{2-} and Fe_3O_4 in this study).

(5) Transport of materials in porous media

Fluids flow through porous rocks and precipitate minerals. Equations describing precipitation in porous medias are listed below:

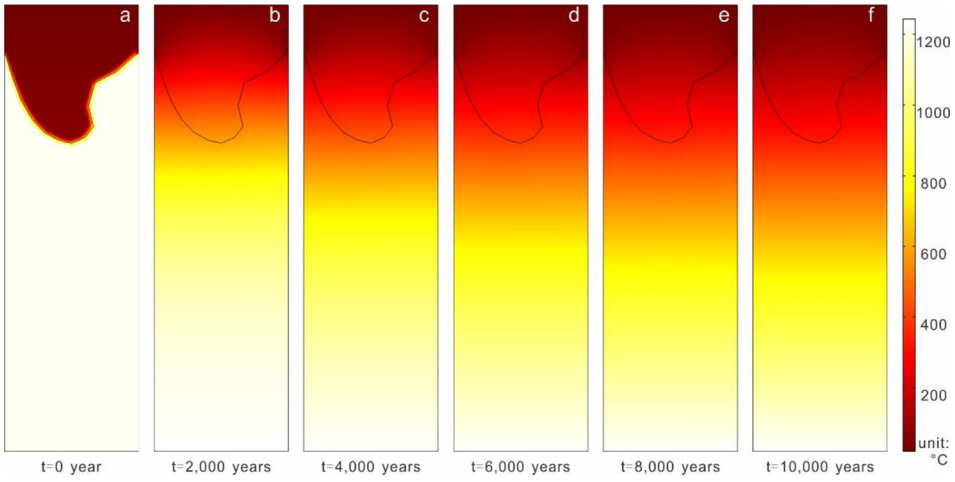

Fig. 8. Diagrams showing variations in the distribution of temperature over time within the entire model.

$$\frac{\partial c_i}{\partial t} + \nabla \cdot (-D_i \nabla c_i) + \nu \cdot \nabla c_i = R_i \tag{13}$$

$$N_i = -D_i \nabla c_i + \nu c_i \tag{14}$$

where c_i is the concentration of each reactant/product in mol/m^3, D_i is the diffusion coefficient of $Fe^{2+/3+}$ and O^{2-} in this study, ν is the velocity of fluids, R_i is reaction rate of the $Fe^{2+/3+}$ and O^{2-}, and N_i is the amount of $Fe^{2+/3+}$ or O^{2-} which participate in chemical reaction, with i and j representing different material participating in the reaction.

4. Results

4.1. Temperature

The distribution of temperature over time within the mineralizing system is shown in Figs. 8 and 9. Temperature is a key control on the distribution of mineralization within magmatic-hydrothermal systems (Li et al., 1979; Zhao et al., 2008, 2009), which means the distribution of temperature can often be used to reflect the distribution of mineralization (Hu et al., 2019, 2020a). The results shown in Figs. 8 and 9 indicate that the area favorable for the generation of mineralization is mainly around the contact between the overlying units and the intrusions, which matches the distribution of mineralization shown in Fig. 4.

4.2. Concentration of IOA mineralization

The distribution of the concentrations of magnetite over time is shown in Fig. 10. Unlike the modified concentration values used in our previous study (in Hu et al., 2020a, concentration is shown in logarithmic form), this paper enhances chemical reaction by setting a customized equilibrium coefficient of reaction to adjust the distribution of concentration value of generated Fe_3O_4 to make it more centralized and closer to geological facts. Thus, the concentration results are

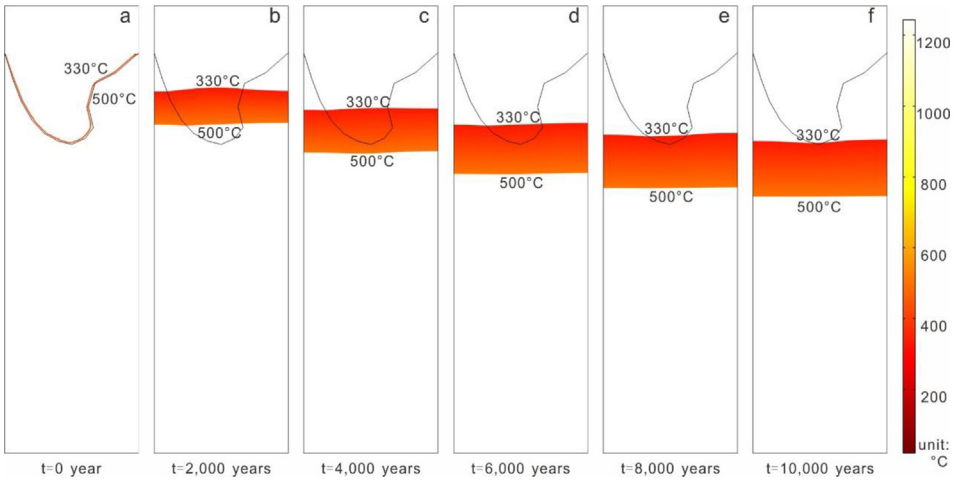

Fig. 9. Diagrams showing variations in the distribution of temperature over time focusing on areas within the temperature range from 330 °C to 500 °C (Li et al., 1979), reflecting the temperature of formation of the IOA-type mineralization within the Yangzhuang deposit.

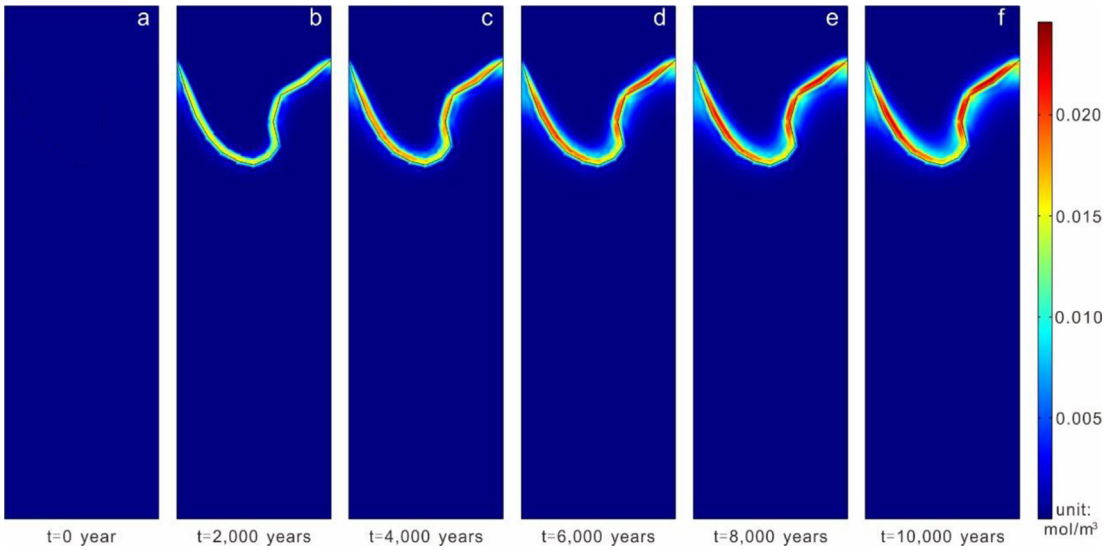

Fig. 10. Diagrams showing the distribution of iron-oxide mineralization (Fe_3O_4) as identified during the modeling undertaken in this study.

shown without any mathematical modification. However, the temperature in our model of the mineralizing system decreases rapidly, causing the rapid cooling and solidification of the peripheral parts of the magma body and hence preventing stoping of mineralization into the magma. The only reasonable explanation for this is therefore the upward migration of the magma body to incorporate part of the overlying units as a large xenolith or inclusion, with mineralization reactions and the replacement of this inclusion or xenolith with IOA mineralization then starting when the rapidly solidifying magma body exsolved fluids at temperatures of 330°C–500 °C. In addition, Fe_3O_4 is generated at the contact between the intrusions and surrounding country rocks, basically matching the fact shown in Fig. 4b, which means its distribution is controlled by the occurrence of the contact of intrusion and Triassic Xujiashan group (Fig. 11).

4.3. Estimation of the duration of ore-forming processes within the Yangzhuang IOA-type magmatic-hydrothermal system

Determining the duration of the mineralizing processes that operated in the study area requires the recording of the value of variables in a specific point in the model. This required the setting of three probes within the middle of the model at depths of −1250 m (P1, in the overlying units), −1350 m (P2, in the contact zone) and −1450 m (P3, in the intrusion; Fig. 12). The values obtained by these probes were automatically recorded during the running of the COMSOL software.

Fig. 13 shows the values of temperatures at the location of the three probes over time. The presence of a heat source at the bottom of the model means that the temperatures of P1 to P3 decrease rapidly but finally become stable at temperatures of 300 °C–400 °C. This high temperature anomaly persists until the cessation of source heating from the bottom of the model when the temperatures then descend to normal geothermal gradients.

Fig. 14 shows the concentrations of reactants and products with Fe_3O_4 concentrations rising rapidly in the first few thousand years before stopping increasing after a period of 8000 years. Previous research, including by numerical modeling, has determined that the processes that form porphyry-type magmatic-hydrothermal deposits persist for <100,000 years (Weis et al., 2012; Hu et al., 2020a). In comparison, the Kiruna-type Yangzhuang deposit appears to have formed much more rapidly, over a duration of perhaps <10,000 years; this may be beyond the precision possible with modern geochronological techniques for at least deposits as old as the Yangzhuang deposit.

5. Discussion

Numerical modeling provides insights into a number of fundamental questions about mineralizing systems (Oliver et al., 2006; Murphy et al., 2008; Eldursi et al., 2010; Ord et al., 2010; Fan et al., 2021; Xiao and Wang, 2021), including the duration and quantification of mineralizing processes (Weis et al., 2012; Zou et al., 2017; Zhao et al., 2018; Hu et al., 2020a). Modern analytical facilities and approaches have enabled research that has determined that a range of mineral deposits form over tens or hundreds of thousands of years or less (Von Quadt et al., 2011; Buret et al., 2016; Large et al., 2018; Li et al., 2018), similar to the durations calculated or estimated using numerical approaches (Weis et al., 2012; Zou et al., 2017; Zhao et al., 2018; Hu et al., 2020a). This initial numerical modeling has been improved by the addition of extra chemical reaction components and improved reaction rate simulations. This has enabled the modeling presented in this study, which suggests that the Yangzhuang Kiruna-type IOA deposit formed rapidly over a period of <10,000 years, with reaction rates decreasing to 0 mol/m^3/year after a period of 8000 years. There are two main controls on this modeled duration. The first is the temperature of the model (Figs. 12 and 13), where temperatures at P1 to P3 almost decrease to the

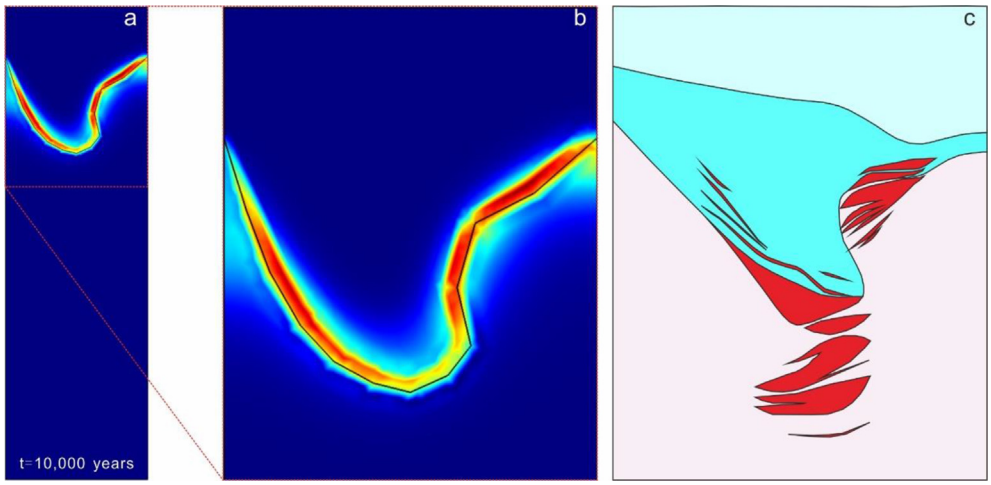

Fig. 11. Comparison of (a) our simulation result, (b) partial zoomed image of Fig. 11a and (c) the cross-section of Fig. 4b.

lower limit of the temperature of the mineralizing system (330 °C), leading to chemical reactions (i.e., magnetite precipitation) at P2 ceasing at this time. The second factor is the diffusion between the overlying country rocks and the intrusion. This is shown in Fig. 14, where the concentration of O^{2-} at P2 reduced to 0 mol/m^3 after 8000 years. However, the concentration of O^{2-} in the background is set as 0.05 mol/m^3, meaning that this O^{2-} cannot rapidly diffuse to the reaction zone at the contact between the country rocks and the intrusion. This indicates that magnetite could be rapidly precipitated in significant amounts in oxygen enriched environments if the intrusion could continuously supply heat as a result of slow cooling (i.e., significantly longer than the duration of the modeled ore-forming processes although this may not result in more magnetite being formed).

Our numerical modeling also provides useful insights into the genesis of the Yangzhuang Kiruna-type IOA deposit. Previous research by Jin (2014) suggested that the mineralization within the intrusion was the result of the stoping of existing mineralization into the magma body, reflecting the higher density of the mineralization (~4.5 t/m^3) relative to the intrusion (~2.6 t/m^3). However, our modeling indicates that this

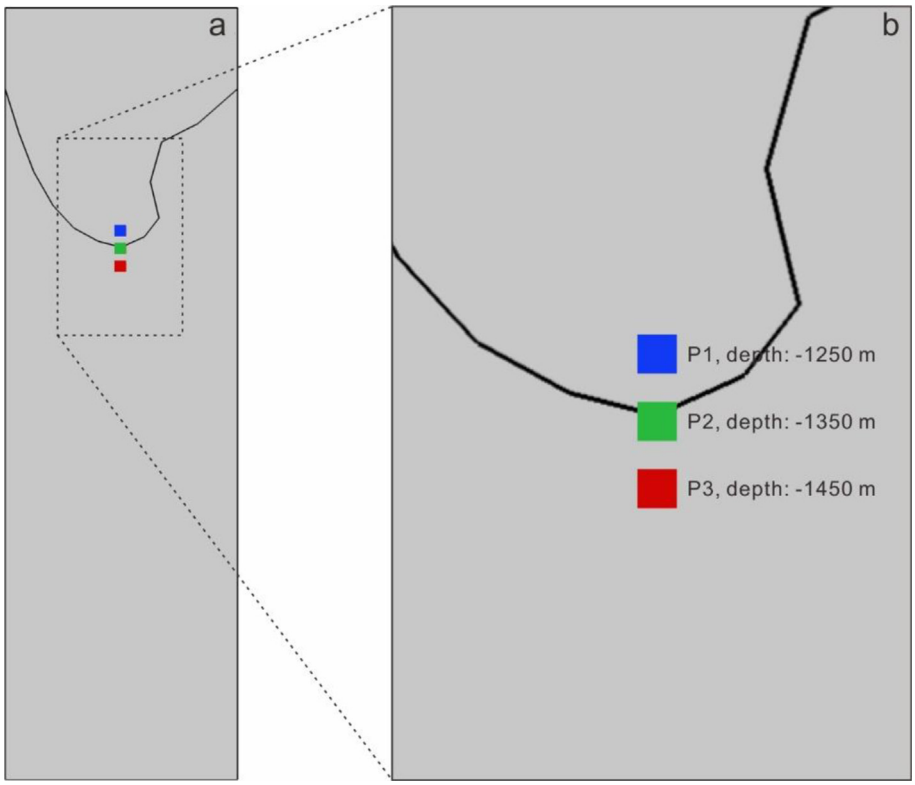

Fig. 12. The locations of the three probes used during this study; see text for details.

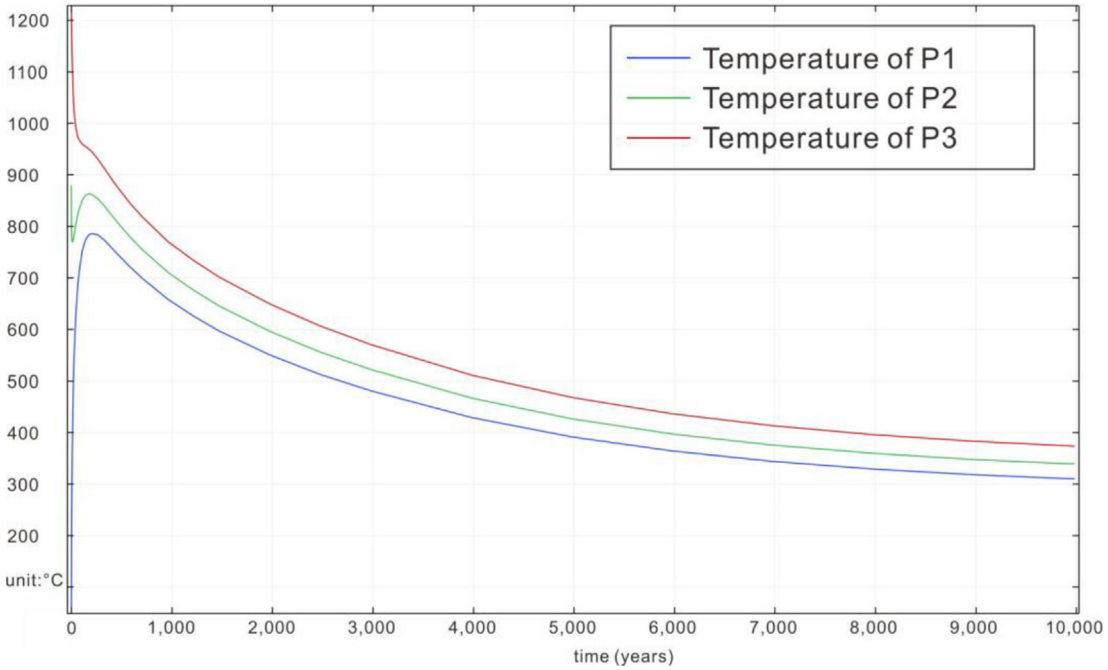

Fig. 13. Diagram showing the values of temperatures of the three probes over time.

may not be the case. Our modeling predicts that mineralization formed outside of the intrusion (see Figs. 4 and 6) but the temperatures obtained from the P3 probe allows the analysis of the genesis of these orebodies. The temperature curve at P3 drops very rapidly over the first 1000 years but not enough IOA mineralization has formed by this stage (Fig. 10). This means that whatever stoped down into the magma was not mineralized before stoping but instead was more likely to be a large section of country rock that either stoped down or was enveloped by ascending magma prior to the exsolution of the magmatic-hydrothermal fluids that formed the mineralization in this area. This is consistent with the 45.75–58.28 wt.% SiO_2 content of the intrusions within the Yangzhuang district (Jin, 2014), indicating that these intermediate-felsic magmas initially cool and solidify at a temperature of ~1000 °C, a temperature that P2 is only at or higher than for a few hundred years. This means if a section of country rocks does not stope down or be enveloped by the magma during this initial period of cooling then it will not be able to enter the magma body. The issue is then the fact that the density of this potentially large xenolith is similar to the density of the magma given that no IOA mineralization has formed at this stage (Table 1). This suggests that the section of country rock might float on top of the magma as a result of the buoyancy force supplied by the latter, although this also precludes any other forces that drive the magma body upwards. The fact that the now mineralized country rock is entirely enclosed by the magma (Fig. 4) suggests the latter, where magmas ascended to surround the country rock, contact metamorphosing and potentially melting the edges of the sedimentary block before the system cooled with the country rock present as an inclusion or xenolith within the cooled and at least semi-solid magma. This magma then exsolved fluids that reacted with the xenolith or inclusion, forming IOA mineralization surrounded by the intrusion as a result of reactions with the $Fe^{2+/3+}$ in the exsolved magmatic-hydrothermal fluid, resulting in the precipitation of magnetite. In summary, although this research has not directly determined the processes that formed the Yangzhuang Kiruna-type IOA deposit, this study validates the use of numerical modeling for furthering our understanding of metallogenic processes and forms the basis of a number of possible routes for future research on the Yangzhuang deposit and beyond.

The numerical simulation modeling undertaken in our study can also provide other insights in addition to examining the duration of mineralizing systems and the genesis of the Yangzhuang deposit. These include the spatial distribution of IOA-type mineralization, fluid flow rates within mineralizing systems, and the nature of chemical reactions. However, our numerical models are admittedly simple, and omit a significant amount of detailed information that could be incorporated in future models. Developing more detailed numerical models will therefore provide deeper insights into processes involved in magma-hydrothermal systems as well as the formation of other types of mineral deposit. However, it should be noted that finite element models (FEM) have several limitations. This includes the fact that our model cannot completely reflect all the coupled processes involved in ore formation, causing minor mismatches between the known data within the Yangzhuang deposit (e.g., the cross-sections, geological reports and other exploration data) and the results of our modeling. In addition, the development of phase change models could enable improved models that can more accurately predict the upward migration and evolution of magma and other processes. We believe these problems could be solved by detailed modification to the calculation approaches.

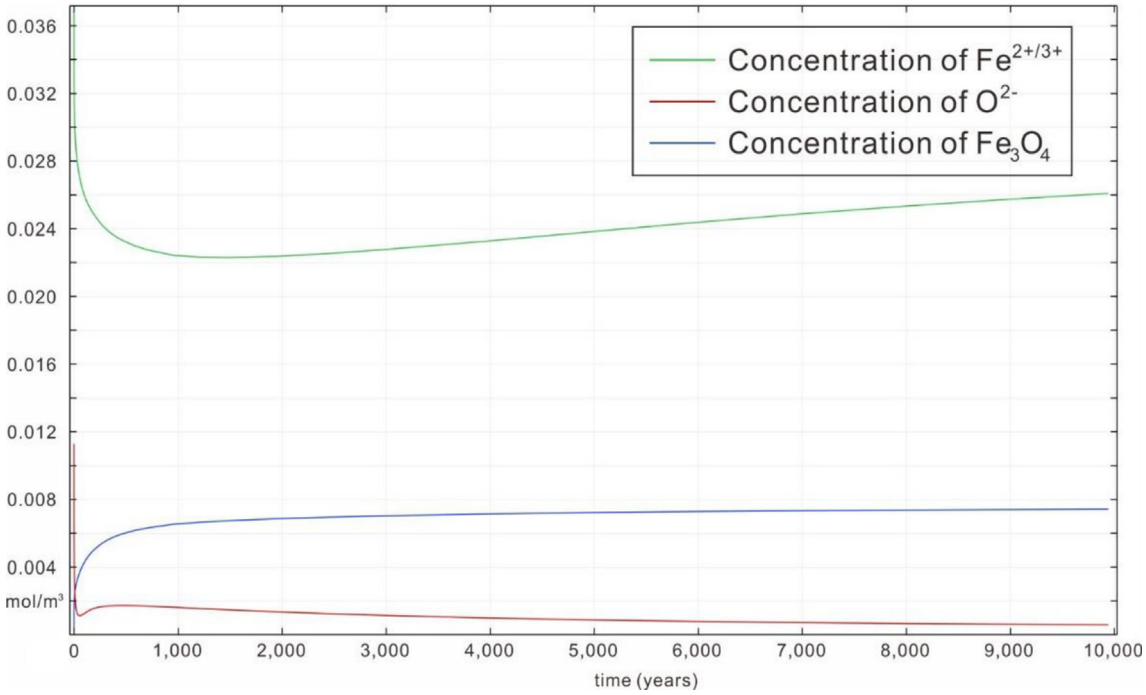

Fig. 14. Diagram showing the concentrations of all three reactants/products at probe location P2 within the modeling undertaken during this study.

Fortunately, the rapid development of computer software and hardware in-depth theoretical studies on the numerical simulation of geological processes means that this problem can be solved soon in the future.

One key problem remaining unsolved is the uncertainty of pre-metallogenic phenomena. As is known to all, the observations of geological phenomena are all post metallogenic. The pre-metallogenic phenomena can only be speculated but not directly measured or tested in laboratories, which caused uncertainty of many boundary conditions. Hence, the simplification of numerical model not only simplified the morphology of geological units, the complexity of geochemical reactions and the coupled relationship of multiple ore-forming processes, but also the boundary conditions (some post metallogenic phenomena are considered as pre-metallogenic phenomena and are used in numerical modeling). Relying on the progresses of analytical methods and geological theories in the future, the uncertainty will be reduced and numerical results will be more convincing on the basis of boundary conditions closer to pre-metallogenic geological facts.

Another problem is that we have developed a 2D model, which means all influences from the two sides of the model are omitted. A 3D model could be used to avoid this problem but importing of a complex 3D model into the COMSOL software is still quite difficult. 3D geological model with random shapes is much more complex than 3D engineering model with regular shapes (e.g., models of plane, bridge and mobile phone) and will generate a large number of fine irregular triangulars, which will shapely increase the amount of calculation and cause the running out of computer memory. Advancements in computer hardwares, softwares, calculation approaches and geological theories will undoubtedly resolve these problems and make numerical simulation more useful in theoretical and practical geological research.

6. Conclusions

This study uses numerical modeling approaches to simulate the forming processes associated with the iron mineralization of the Yangzhuang Kiruna-type IOA deposit, obtaining the following results:

(1) Our numerical modeling coupled pressure, heat transfer, fluid-flow, chemical reaction and material migration and successfully gave numerical explanation to questions related to genesis of the Yangzhuang kiruna-type iron deposit, which expanded the usage of numerical modeling approach within geological research. The results show that temperature and structure (occurrence of the contact of intrusion and the Triassic Xujiashan group) are factors which control the formation of the Yangzhuang deposit.
(2) The modeled distribution of temperature and the concentration of reactants/products of the chemical reactions involved in Kiruna-type IOA mineralization indicates that these deposits can form rapidly over periods of <10,000 years, with the reaction stops after 8000 years, which is more rapid than previously thought.
(3) The orebodies within the intrusion did not form by the stoping of mineralization into the intrusion. Instead, the predicted temperatures and the concentration of magnetite over time suggests that the magma ascended and upwelled around a block of country rock, forming a xenolith or inclusion that was then mineralized by interaction with fluids exsolved from the magma.
(4) The simulation approach used in our research has several limitations. Future development into both theories and methods will definitely improve the practical significance of numerical simulation of ore-forming processes and provide quantitative results for more geological issues.

Credit authorship contribution statement

Xunyu Hu: Conceptualization, interpretation of data and writing. Simon Jowitt: writing, editing and interpretation of data. Feng Yuan: Funding acquisition. Jinhui Luo: Data processing. Yuhua Chen: review & editing. Hui Yang: Funding acquisition. Keyue Ren: Conceptualization. Yongguo Yang: Funding acquisition.

Declaration of competing interest

The authors declare that they have no known competing financial interests or personal relationships that could have influenced the work reported in this paper.

Acknowledgements

This research was financially supported by funds from the National Natural Science Foundation of China (Grant No. 41820104007, 41872248, 41971335, 51978144), A Project Funded by the Priority Academic Program Development of Jiangsu Higher Education Institutions (PAPD) and China Scholarship council. We also would like to thank our project partners Mineral Explorating and Developing Bureau of Eastern China for providing geological data and the Geological Exploration Technologies Institute of Anhui Province for assistance throughout this research. We also thank Miss Shasha Xu and Miss Ting Zhang for their help during the drafting of this manuscript.

References

Anderson, D.L., 1989. Theory of the Earth. Blackwell scientific publications.
Bickle, M.J., 1978. Heat loss from the Earth: a constraint on Archaean tectonics from the relation between geothermal gradients and the rate of plate production. Earth Planet. Sci. Lett. 40 (3), 301–315.
Buret, Y., von Quadt, A., Heinrich, C., Selby, D., Wälle, M., Peytcheva, I., 2016. From a long-lived upper-crustal magma chamber to rapid porphyry copper emplacement: reading the geochemistry of zircon crystals at Bajo de la Alumbrera (NW Argentina). Earth Planet Sci. Lett. 450, 120–131.
Chai, F., Yang, F., Liu, F., Santosh, M., Geng, X., Li, Q., Liu, G., 2013. The Abagong apatite-rich magnetite deposit in the Chinese Altay Orogenic Belt: a Kiruna-type iron deposit. Ore Geol. Rev. 57, 482–497.
Chang, Y., Liu, X., Wu, Y., 1991. The Copper-Iron Belt of the Lower and Middle Reaches of the Changjiang River. Geological Publishing House, Beijing.
Chen, Y., Sun, G., Zhao, Q., 2021. Distance anomaly factors for gold potential mapping in the Jinchanggouliang area, Inner Mongolia, China. Earth Sci. Inf. 2021 (11).
Cheng, Q., 2021. What are Mathematical Geosciences and its frontiers? Earth Sci. Front. 28 (3), 6–25.
Eldursi, K., Branquet, Y., Guillou-Frottier, L., Marcoux, E., 2009. Numerical investigation of transient hydrothermal processes around intrusions: heat-transfer and fluid-circulation controlled mineralization patterns. Earth Planet Sci. Lett. 288 (1–2), 70–83.
Esmailiy, D., Zakizadeh, S., Sepidbar, F., Kanaanian, A., Niroomand, S., 2016. The shaytor apatite-magnetite deposit in the kashmar-kerman tectonic zone (Central Iran): a kiruna-type iron deposit. Open J. Geol. 6 (8), 895–910.
Fan, X., Hu, Z., Xu, S., Chen, C., Yi, N., 2021. Numerical simulation study on ore-forming factors of the Gejiu ore deposit, China. Ore Geol. Rev. 135 (11), 104209.
Förster, H., Knittel, U., 1979. Petrographic observation on a magnetite deposit at Mishdovan, Central Iran. Econ. Geol. 74, 1485–1489.
Frietsch, R., Perdahl, J.A., 1995. Rare earth elements in apatite and magnetite in Kiruna-type iron ores and some other iron ore types. Ore Geol. Rev. 9 (6), 489–510.
Gorczyk, W., Vogt, K., 2015. Tectonics and melting in intra-continental settings. Gondwana Res. 27 (1), 196–208.
Gorczyk, W., Hobbs, B., Gessner, K., Gerya, T., 2013. Intracratonic geodynamics. Gondwana Res. 24 (3–4), 838–848.
Hart, B.S., Flemings, P.B., Deshpande, A., 1995. Porosity and pressure: role of compaction disequilibrium in the development of geopressures in a Gulf Coast Pleistocene basin. Geology 23 (1), 45–48.
Heidarian, H., Alirezaei, S., Lentz, D.R., 2017. Chadormalu Kiruna-type magnetite-apatite deposit, Bafq district, Iran: insights into hydrothermal alteration and petrogenesis from geochemical, fluid inclusion, and sulfur isotope data. Ore Geol. Rev. 83, 43–62.
Hobbs, B., Regenauer-Lieb, K., Ord, A., 2007. Thermodynamics of folding in the middle to lower crust. Geology 35 (2), 175–178.
Hou, T., Zhang, Z., Du, Y., 2010. Deep ore magma-hydrothermal system of Zhonggu ore field in southern part of Ningwu Basin. Earth Sci. Front. 17, 186–194.
Hou, T., Zhang, Z.C., Kusky, T., 2011. Gushan magnetite–apatite deposit in the Ningwu Basin, lower Yangtze River valley, SE China: hydrothermal or kiruna-type? Ore Geol. Rev. 43, 333–346.
Hu, B., Wang, F., Sun, Z., Liu, C., Bai, L., 2003. The pressure gradient in the lithosphere. Earth Sci. Front. 10 (3), 129–133.
Hu, X., Yuan, F., Li, X., Jowitt, S.M., Jia, C., Zhang, M., Zhou, T., 2018. 3D characteristic analysis-based targeting of concealed kiruna-type fe oxide-apatite mineralization within the yangzhuang deposit of the zhonggu orefield, southern ningwu volcanic basin, middle-lower yangtze river metallogenic belt, China. Ore Geol. Rev. 92, 240–256.
Hu, X., Chen, Y., Liu, G., Yang, H., Luo, J., Ren, K., Yang, Y., 2022. Numerical modeling of formation of the Maoping Pb-Zn deposit within the Sichuan-Yunnan-Guizhou Metallogenic Province, Southwestern China: implications for the spatial distribution of concealed Pb mineralization and its controlling factors. Ore Geol. Rev. 2022, 104573 (in press).
Hu, X., Li, X., Yuan, F., Jowitt, S.M., Ord, A., Li, Y., Dai, W., Ye, R., Zhou, T., 2019. Numerical simulation based targeting of the magushan skarn Cu–Mo deposit, middle-lower yangtze metallogenic belt, China. Minerals 9 (10), 588.
Hu, X., Li, X., Yuan, F., Ord, A., Jowitt, S.M., Li, Y., Dai, W., Zhou, T., 2020a. Numerical modeling of ore-forming processes within the chating Cu-Au porphyry-type deposit, China: implications for the longevity of hydrothermal systems and potential uses in mineral exploration. Ore Geol. Rev. 116, 103230, 2020.
Hu, X., Li, X., Yuan, F., Jowitt, S.M., Ord, A., Ye, R., Li, Y., Dai, W., Li, X., 2020b. 3D numerical simulation-based targeting of skarn type mineralization within the Xuancheng-magushan orefield, middle-lower yangtze metallogenic belt, China. Lithosphere 2020 (1), 1–20.
Jia, C., Yaun, F., Li, X., Hu, X., Liao, B., Sun, W., Zhang, M., Shen, Le, 2018. Metallogenic dynamics simulation based on multi-source data constraint: a case study of the typical deposit in Zhongu ore field in Ningwu Basin. Chin. J. Geol. 53 (4), 1327–1346.
Jin, M., 2014. On geological and geochemical characteristics and genesis of iron deposit in Yangzhuang of Dangtu in Anhui. J. Geol. 38 (2), 206–218.
Kumar, A., Pramanik, S., Mishra, M., 2016. COMSOL Multiphysics® Modeling in Darcian and Non-Darcian Porous Media. 2016 COMSOL Conference, Bangalore, India.
Large, S.J., Quadt, A.V., Wotzlaw, J.F., Guillong, M., Heinrich, C.A., 2018. Magma evolution leading to porphyry Au-Cu mineralization at the Ok Tedi deposit, Papua New Guinea: trace element geochemistry and high-precision geochronology of igneous zircon. Econ. Geol. 113 (1), 39–61.
Li, Z., Xu, Z., 2015. Dynamics of along-strike transition between oceanic subduction and continental collision: effects of fluid-melt activity. Acta Petrol. Sin. 31 (12), 3524–3530.
Li, Y., Wei, J., Zhou, X., Ma, X., 1979. Some features of the fluid inclusions and the ore-forming temperature of a certain porphyrite-type iron deposit. Acta Geologica Sinca 1, 50–59.

Li, X., Yuan, F., Zhang, M., Jia, C., Jowitt, S.M., Ord, A., Zheng, T., Hu, X., Li, Y., 2015. Three-dimensional mineral prospectivity modeling for targeting of concealed mineralization within the Zhonggu iron orefield, Ningwu Basin, China. Ore Geol. Rev. 71, 633–654.
Li, Y., Li, X.H., Selby, D., Li, J.W., 2018. Pulsed magmatic fluid release for the formation of porphyry deposits: tracing fluid evolution in absolute time from the Tibetan Qulong Cu-Mo deposit. Geology 46 (1), 7–10.
Li, X., Yuan, F., Zhang, M., Jowitt, S.M., Ord, A., Zhou, T., Dai, W., 2019. 3D computational simulation-based mineral prospectivity modeling for exploration for concealed Fe–Cu skarn-type mineralization within the Yueshan orefield, Anqing district, Anhui province, China. Ore Geol. Rev. 105, 1–17.
Li, S., Chen, J., Liu, C., Wang, Y., 2021. Mineral prospectivity prediction via convolutional neural networks based on geological big data. J. Earth Sci. (English Edition) 32 (2), 327–347.
Lister, C.R.B., 1963. Geothermal gradient measurement using a deep sea corer. Geophys. J. Int. 7 (5), 571–583.
Liu, Y., Dai, T., 2014. Numerical modeling of pore-fluid flow and heat transfer in the Fushan iron ore district, Hebei, China: implications for hydrothermal mineralization. J. Geochem. Explor. 144, 115–127.
Liu, L., Zhao, Y., Zhao, C., 2010a. Coupled geodynamics in the formation of Cu skarn deposit in Tongling-Anqing district, China: computational modeling and implications for exploration. J. Geochem. Explor. 106, 146–155.
Liu, L., Zhou, R., Zhao, C., 2010b. Constraints of tectonic stress regime on mineralization system related to the hypabyssal intrusion: implication from the computational modeling experiments on the geodynamics during cooling process of the Yuenshan intrusion in Anqing district, China. Acta Petrol. Sin. 26, 2869–2878.
Liu, L., Wan, C., Zhao, Y., 2011. Geodynamic constraints on orebody localization in the Anqingorefield, China: computational modeling and facilitating predictive exploration of deep deposits. Ore Geol. Rev. 43, 249–263.
Liu, Y., Xia, Q., Cheng, Q., 2021. Aeromagnetic and geochemical signatures in the Chinese western Tianshan: implications for tectonic setting and mineral exploration. Nat. Resor. Res. (3–4).
Mandl, G.M., 1988. Mechanics of Tectonic Faulting. Elsevier, Amsterdam.
Mao, X., Zhang, W., Liu, Z., Ren, J., Deng, H., 2020. 3D mineral prospectivity modeling for the low-sulfidation epithermal gold deposit: a case study of the Axi gold deposit, western Tianshan, NW China. Minerals 10 (3).
Murphy, F.C., Ord, A., Hobbs, B.E., Willetts, G., Barnicoat, A.C., 2008. Targeting stratiform Zn-Pb-Ag massive sulfide deposits in Ireland through numerical modeling of coupled deformation, thermal Transport, and fluid flow. Econ. Geol. 103, 1437–1458.
Mineral Explorating and Developing Bureau of Eastern China, 2011. Geological Report on the Yangzhuang Deposit, 1–246 (Internal data).
Ningwu Research Group, 1978. Ningwu Porphyry Iron Ores. Geological Publishing House, Beijing (in Chinese).
Nyström, J., Henriquez, E., 1994. Magmatic features of iron ores of the Kiruna type in Chile and Sweden: ore textures and magnetite geochemistry. Econ. Geol. 89, 820–839.
Oliver, N.H., McLellan, J.G., Hobbs, B.E., Cleverley, J.S., Ord, A., Feltrin, L., 2006. Numerical models of extensional deformation, heat transfer, and fluid flows across basement-cover interfaces during basin-related mineralization. Econ. Geol. 101, 1–31.
Ord, A., Hobbs, E.B., Zhao, C., 2010. Theoretical and numerical investigation into roles of geofluid flow in ore forming systems: integrated mass conservation and generic model approach. J. Geochem. Explor. 106, 251–260.
Ord, A., Hobbs, B.E., Lester, D.R., 2012. The mechanics of hydrothermal systems: I. Ore systems as chemical reactors. Ore Geol. Rev. 49, 1–44.
Pirajno, F., Zhou, T., 2015. Intracontinental porphyry and porphyry skarn mineral systems in eastern China: scrutiny of a special case “made-in-China”. Econ. Geol. 110 (3), 603–629.
Porwal, A., Carranza, E.J.M., 2015. Introduction to the Special Issue: GIS-based mineral potential modelling and geological data analyses for mineral exploration. Ore Geol. Rev. 71, 477–483.
Rojas, P.A., Barra, F., Deditius, A., Reich, M., Simon, A., Roberts, M., Rojo, M., 2018. New contributions to the understanding of kiruna-type iron oxide-apatite deposits revealed by magnetite ore and gangue mineral geochemistry at the el romeral deposit, Chile. Ore Geol. Rev. 93, 413–435.
Sillitoe, R.H., Burrows, D.R., 2002. New field evidence bearing on the origin of the El Laco magnetite deposit, Northern Chile. Econ. Geol. 97, 1101–1109.
Sun, T., Chen, F., Zhong, L., Liu, W., Wang, Y., 2019. GIS-based mineral prospectivity mapping using machine learning methods: a case study from Tongling ore district, eastern China. Ore Geol. Rev. 109, 26–49.
Sun, T., Li, H., Wu, K., Chen, F., Hu, Z., 2020. Data-driven predictive modelling of mineral prospectivity using machine learning and deep learning methods: a case study from southern Jiangxi province, China. Minerals 10 (2), 102.
Tang, Y., 1998. Geology of Copper-Gold Polymetallic Deposits in the Along-Chang Jiang Area of Anhui Province. Geological Publishing House, Beijing.
Von Quadt, A., Erni, M., Martinek, K., Moll, M., Peytcheva, I., Heinrich, C.A., 2011. Zircon crystallization and the lifetimes of ore-forming magmatic-hydrothermal systems. Geology 39 (8), 731–734.
Wang, Y., Zhang, Q., Wang, Y., 2001. Geochemical characteristics of volcanic rocks from Ningwu area, and its significance. Acta Petrol. Sin. 17, 565–575.
Weis, P., Driesner, T., Heinrich, C.A., 2012. Porphyry-copper ore shells form at stable pressure-temperature fronts within dynamic fluid plumes. Science 338 (6114), 1613–1616.
Xiao, F., Wang, K., 2021. Fault and intrusion control on copper mineralization in the Dexing porphyry copper deposit in Jiangxi, China: a perspective from stress deformation-heat transfer-fluid flow coupled numerical modeling. Earth Sci. Front. 28 (3), 190–207.
Zhai, Y., 1992. Metallogenic Regularity of Iron and Copper (Gold) Deposits in the Middle and Lower Valley of the Yangtze River. Geological Publishing House, Beijing.
Zhang, S., Carranza, E., Wei, H., Xiao, K., Xu, Y., 2021. Data-driven mineral prospectivity mapping by joint application of unsupervised convolutional auto-encoder network and supervised convolutional neural network. Nat. Resor. Res. 1.
Zhao, C., 2015. Advances in numerical algorithms and methods in computational geosciences with modeling characteristics of multiple physical and chemical processes. Sci. China(Technol. Sci.) 58, 783–795.
Zhao, C., 2016. Computational methods for simulating some typical problems in computational geosciences. Int. J. Comput. Methods 13, 1–17.
Zhao, C., Hobbs, B.E., Ord, A., Hornby, P., Peng, S., 2008. Morphological evolution of three-dimensional chemical dissolution front in fluid-saturated porous media: a numerical simulation approach. Geofluids 8 (2), 113–127.
Zhao, C., Hobbs, B.E., Ord, A., 2009. Fundamentals of Computational Geoscience: Numerical Methods and Algorithms. Springer, Berlin.
Zhao, C., Hobbs, B.E., Ord, A., 2018. Modeling of mountain topography effects on hydrothermal pb-zn mineralization patterns: generic model approach. J. Geochem. Explor. 199, 400–410.
Zhao, X., Zeng, L., Liao, W., Li, W., Hu, H., Li, J., 2020. An overview of recent advances in porphyrite iron (iron oxide- apatite, IOA) deposits in the Middle-Lower Yangtze River Valley Metallogenic Belt and its implication for ore genesis. Earth Sci. Front. 27 (2), 197–217, 2020.
Zhou, T., Wang, S., Fan, Y., Yuan, F., Zhang, D., White, N.C., 2015. A review of the intracontinental porphyry deposits in the Middle-Lower Yangtze River Valley metallogenic belt, Eastern China. Ore Geol. Rev. 65, 433–456.
Zhou, T., Fan, Y., Chen, J., Xiao, X., Zhang, S., 2020. Critical metal resources in the middle-lower Yangtze River vally metallogenic belt. Chin. Sci. Bull. 65 (33), 3665–3677.
Zhu, J., Chen, J., 2019. Research status of FLAC3D-based mineralization process simulation. J. Geol. 43 (3), 506–513.
Zou, Y., Liu, Y., Dai, T., Mao, X., Lei, Y., Lai, J., Tian, H., 2017. Finite difference modeling of metallogenic processes in the Hutouya Pb-Zn deposit, Qinghai, China: implications for hydrothermal mineralization. Ore Geol. Rev. 91, 463–476.
Zuo, R., Kreuzer, O.P., Wang, J., Xiong, Y., Zhang, Z., Wang, Z., 2021. Uncertainties in gis-based mineral prospectivity mapping: key types, potential impacts and possible solutions. Nat. Resor. Res. 1–21.